

Article

Single-Molecule Observation of the Intermediates in a Catalytic Cycle

William J Ramsay, Nicholas A W Bell, Yujia Qing, and Hagan Bayley

J. Am. Chem. Soc., **Just Accepted Manuscript** • DOI: 10.1021/jacs.8b09282 • Publication Date (Web): 26 Nov 2018

Downloaded from <http://pubs.acs.org> on November 26, 2018

Just Accepted

“Just Accepted” manuscripts have been peer-reviewed and accepted for publication. They are posted online prior to technical editing, formatting for publication and author proofing. The American Chemical Society provides “Just Accepted” as a service to the research community to expedite the dissemination of scientific material as soon as possible after acceptance. “Just Accepted” manuscripts appear in full in PDF format accompanied by an HTML abstract. “Just Accepted” manuscripts have been fully peer reviewed, but should not be considered the official version of record. They are citable by the Digital Object Identifier (DOI®). “Just Accepted” is an optional service offered to authors. Therefore, the “Just Accepted” Web site may not include all articles that will be published in the journal. After a manuscript is technically edited and formatted, it will be removed from the “Just Accepted” Web site and published as an ASAP article. Note that technical editing may introduce minor changes to the manuscript text and/or graphics which could affect content, and all legal disclaimers and ethical guidelines that apply to the journal pertain. ACS cannot be held responsible for errors or consequences arising from the use of information contained in these “Just Accepted” manuscripts.

Single-Molecule Observation of the Intermediates in a Catalytic Cycle

William J. Ramsay, Nicholas A. W. Bell, Yujia Qing, Hagan Bayley*

University of Oxford, Chemistry Research Laboratory, Oxford, OX1 3TA, UK

ABSTRACT: The development of catalysts benefits from knowledge of the intermediate steps that accelerate the transformations of substrates into products. However, key transient species are often hidden in ensemble measurements. Here, we show that a protein nanoreactor can sample the intermediate steps in a catalytic cycle by the continuous single-molecule observation of a stoichiometric reaction in solution. By monitoring changes in the flow of ionic current through an α -hemolysin protein pore, we observed three intermediate metal-ligand complexes in a gold(I)-catalysed reaction that converts an acetylenic acid to an enol lactone, revealing a transitional coordination complex that had been previously unobserved. A kinetic isotope effect helped assign the various metal-ligand species. Measurements of the lifetimes of the intermediates allowed a full kinetic analysis of the metal-catalysed reaction cycle.

INTRODUCTION

Chemical reactions catalysed by metals provide access to valuable pharmaceuticals¹ and fine chemicals.² The control over bond-breaking and bond-forming processes during metal-catalysed reactions³ requires awareness of the intermediate metal-ligand species⁴⁻⁵ that mediate the conversion of substrates into products.⁶ This critical information is restricted by the limited number of techniques to monitor transient species continuously with molecular resolution.⁷⁻¹¹ Although single-molecule fluorescence microscopy has enabled the investigation of the initiation dynamics of a surface-supported palladium catalyst,¹²⁻¹⁴ the resolution of the multiple kinetic steps involved in a catalytic cycle remains elusive. The nanoreactor approach used here is a versatile technique to observe the kinetics of transient intermediates at the single-molecule level.

The staphylococcal α -hemolysin (α HL) transmembrane pore (Figure 1a)¹⁵ has been used as a nanoreactor¹⁶ to monitor a variety of chemistries at the single-molecule level, including metal ion chelation,¹⁷ the detection of metal-coordinating neurotransmitters,¹⁸ a kinetic isotope effect,¹⁹⁻²⁰ Cu(I)-catalyzed azide-alkyne cycloaddition,²¹ and the continuous, stochastic movement of a small-molecule walker along a five-foothold track.²² Here, we use the α HL nanoreactor to examine a metal-catalysed reaction (Figure 1b). The lumen of an α HL pore was genetically engineered to accommodate the binding of a single, catalytically active Au^I metal ion, which binds to alkyne substrates (Figure 1c), and can catalytically cyclise acetylenic acids to enol lactones (Figure 1d).²³⁻

25

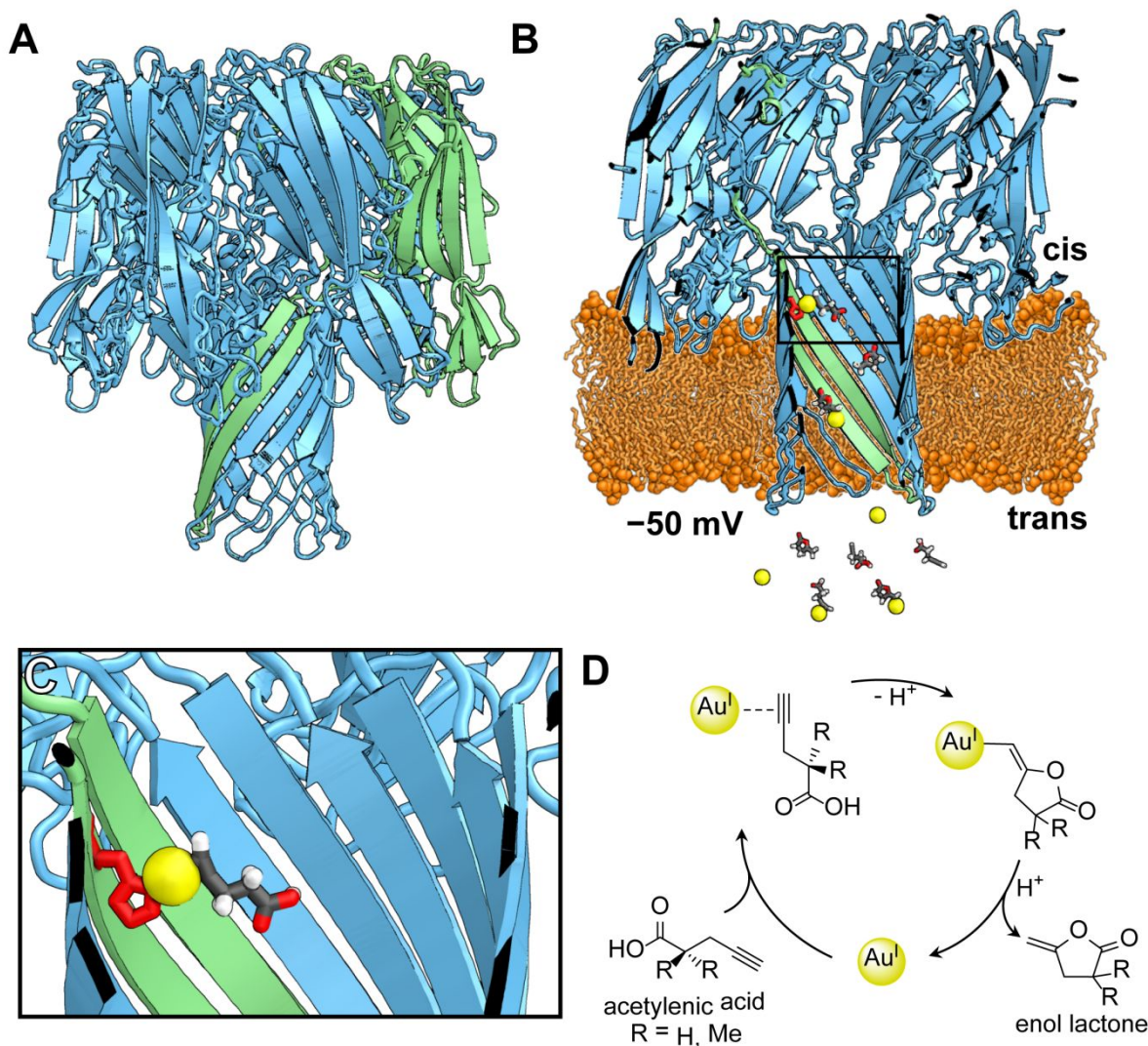


Figure 1. The P_H α HL pore: a nanoreactor for the investigation of Au^I catalysis. **(a)** WT α HL (PDB code 7AHL) is a mushroom-shaped transmembrane protein pore comprising seven identical subunits. A side view of the ribbon structure shown with one of the subunits highlighted in green. **(b)** A sagittal section of the engineered α HL pore, P_H , embedded in a planar lipid bilayer (orange) for single-channel electrical recording. P_H contains one subunit with a histidine substitution at position 145 (red in stick representation). The side chain of His-145 points into the lumen of the transmembrane β barrel and can coordinate metal-ligand complexes from solution, entering from the *trans* compartment. **(c)** An expanded view around His-145, with bound 4-pentynoic acid: Au^I (yellow sphere), 4-pentynoic acid (stick representation: carbon, grey; hydrogen, white; oxygen, red). **(d)** The proposed catalytic cycle for transformation of an acetylenic acid to an enol lactone.

In our study, the modified α HL pore serves as a sensing platform; the catalytic transformation of acetylenic acids predominantly occurs in solution, while the pore samples the intermediate metal-ligand species that are involved in the reaction and records the interconversions of each intermediate. Continuous monitoring over the course of the reaction allows the assembly of information connecting catalytic steps and thereby the construction of **a catalytic cycle in accord with our single-molecule observations**. Our approach suggests a general method to follow metal-catalysed aqueous reactions.

RESULTS & DISCUSSION

Gold(I) binding to the synthetic pore.

Before investigating the Au^I catalysed reaction, we examined the binding of Au^I and Au^I-alkyne complexes to the nanopore. We used a histidine-containing α HL pore to determine the binding kinetics of Au^I with an imidazole group at 21 ± 1 °C (Figure 2a). The same pore was subsequently used to study Au^I catalysis. A mutant α HL monomer, T145H, was assembled together with wild-type (WT) subunits, and the heteroheptameric pore (WT)₆(T145H)₁ (referred to as P_H) was purified by SDS-polyacrylamide gel electrophoresis (Supplementary Section 1.2, Figure S1). The histidine substitution at position 145 in P_H orientates the imidazole side-chain into the lumen of the β barrel, where it can coordinate to a single Au^I cation (none of the natural His residues in the protein are in the conductive pathway, Figure S2). The amplitude of the metal-binding events was enhanced by positioning the coordinating ligand near the pore constriction.²⁶ P_H was characterised by current recording in planar lipid bilayers and carried a single-channel current of -76.6 ± 2.1 pA at -50 mV in 2 M KCl, 10 mM 2-(*N*-morpholino)ethanesulfonic acid (MES), pH 6.1 ($n = 25$; Table S1). The addition of gold(I) chloride to the *trans* compartment resulted in the fluctuation of the ionic current between two discrete levels separated by $\Delta I = 1.10 \pm 0.07$ pA (Figure 2b), where ΔI is the difference between the current carried by the unoccupied pore (P_H) and that of the pore with bound Au^I (P_H·Au^I), i.e. metal binding results in an increase in the unitary conductance of the pore.¹⁸ Although metal binding to modified α HL pores has been observed to both induce and block the flow of current, the subtle reasons behind this phenomenon have yet to be elucidated. The dominant gold species in 2 M KCl at pH 6.1 and 21 ± 1 °C in the binding experiments is the linear molecule Au^ICl₂⁻, as the gold concentrations (≤ 5 μ M) are well below the isoactivity boundary between Au^ICl₂⁻ and Au^{III}Cl₄⁻ and disproportionation to Au^{III} and Au⁰ is negligible.²⁷⁻²⁸ The events associated with Au^I binding had a mean lifetime (τ_{off}) of 2.1 ± 0.2 s and were not seen with WT₇ pores (Figure S11). By assuming that the Au^ICl₂⁻ concentration inside the pore equals that in solution,¹⁶ we performed a kinetic analysis of the events, and deduced that the histidine residue and Au^I reversibly form a binary complex (Figure 2c, top). The reciprocal of the mean inter-event interval (τ_{on}) is proportional to the Au^ICl₂⁻ concentration, which is consistent with a bimolecular interaction for which $1/\tau_{\text{on}} = k_{\text{on}}[\text{Au}^{\text{I}}\text{Cl}_2^-]$. In contrast, a plot of the reciprocal of the mean lifetime of the complex (τ_{off}) versus the Au^ICl₂⁻ concentration has a near zero slope (Figure 2c, bottom), which is consistent with a unimolecular dissociation mechanism ($1/\tau_{\text{off}} = k_{\text{off}}$). The values of τ_{on} and τ_{off} were determined by fitting dwell-time histograms for each Au^ICl₂⁻ concentration to single exponential functions. The forward ($k_{\text{on}} = 1.52 \pm 0.05 \times 10^6$ M⁻¹s⁻¹) and reverse ($k_{\text{off}} = 0.49 \pm 0.05$ s⁻¹) rate constants derived from the τ values yield an equilibrium

association constant of Au^I to imidazole of $K_a = 3.1 \pm 0.3 \times 10^6 \text{ M}^{-1}$ ($n = 4$, independent experiments).

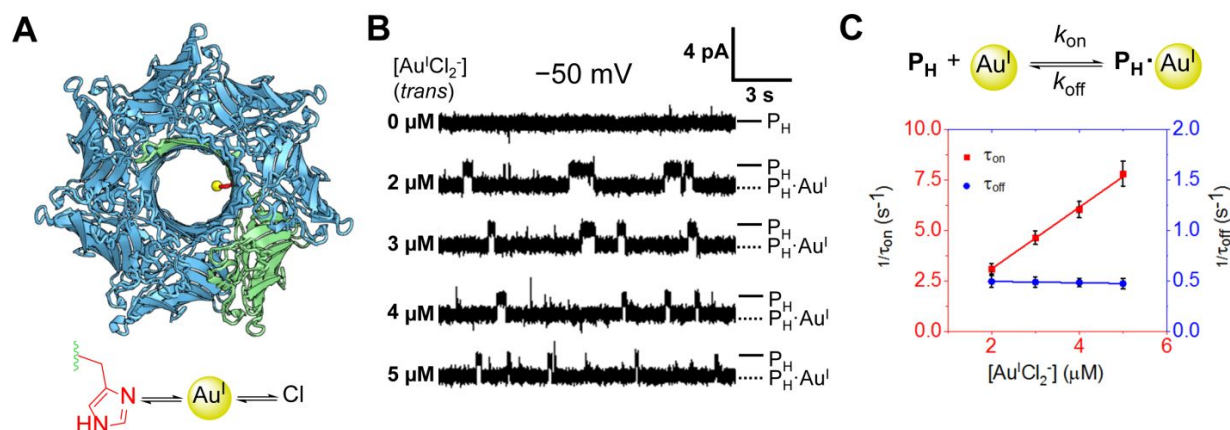


Figure 2. The P_H pore binds Au^I. (a) Ribbon representation of the P_H pore viewed from the bottom of the β barrel. The single histidine side chain (red) binds Au^I (yellow sphere) reversibly. (b) Single-channel recordings at -50 mV with 2 M KCl, 10 mM MES (pH 6.1) in both compartments, and 0 to 5 μM Au^ICl₂⁻ in the trans compartment. The two current levels correspond to the unoccupied pore (P_H) and to the pore with Au^ICl₂⁻ bound to the histidine residue (P_H·Au^I). (c) Proposed kinetic scheme describing Au^I binding to the P_H pore and plots of the reciprocals of the mean inter-event intervals (τ_{on}) and the dwell times of Au^I (τ_{off}) versus the Au^ICl₂⁻ concentration.

We also prepared the phosphine-coordinated Au^I-complex chloro(*tris*(2-carboxyethyl)phosphine) gold(I) (Au^I(tcep)Cl) *in situ* by mixing chloro(tetrahydrothiophene) gold(I) (Au^I(tht)Cl) with TCEP (*tris*(2-carboxyethyl)phosphine) (Supplementary Section 1.4). Phosphine ligated Au^I-complexes are commonly used as catalysts to activate alkenes and alkynes,²⁹⁻³¹ where the phosphine ligand engenders solubility to a discrete Au^I complex. In order to follow the Au^I-catalysed cyclisation of acetylenic acids at the single-molecule level, we found that the use of Au^I(tcep)Cl was a necessity (see below). Although we observed TCEP coordination to Au^ICl₂⁻ in 2 M KCl solutions by ³¹P{¹H} NMR spectroscopy (Figure S4), in single-molecule experiments, we did not observe blocking events consistent with the coordination of TCEP (or THT) to Au^I bound to His-145 when Au^I(tcep)Cl was added to the *trans* compartment (Figures S12 and S13). Rather, we observed fluctuations in the ionic current consistent with Au^ICl₂⁻ binding that occurs from the ligand exchange of Au^I(tcep)Cl in 2 M KCl solution (Table S2 and Supplementary Section 2.3). Thus, although Au^I(tcep)Cl is present in solution, we did not have to consider events associated with TCEP binding to P_H-bound Au^I when we used Au^I(tcep)Cl in our alkyne binding and catalytic investigations. We postulate that the dwell time, τ_{off}, of TCEP bound to a Au^I ion bound to P_H is beyond the resolution of the experiment, perhaps exacerbated by the *trans* influence of the imidazole coordinating group.³²

Alkyne Binding to gold(I)

A key, first step in homogeneous Au^I-catalysed reactions of alkynes is the formation of a Au^I-alkyne π -complex, in which the alkyne binds side-on to a single Au^I centre (Figure 1d).³³⁻³⁶ Before investigating a Au^I catalysed reaction, we sought to detect this binding behaviour at the single-molecule level. We prepared a series of alkyne esters (**1** – **3**; Figure 3, a to c), which can coordinate to but not react on Au^I, and investigated their binding behaviour to Au^I and the histidine pore P_H. Alkyne-ester **1** and Au^I(tcep)Cl were mixed in a 1:1 ratio and added to the *trans* compartment of the recording apparatus at –50 mV in 2 M KCl, 10 mM MES, pH 6.1. NMR spectroscopy confirmed that these components do not react³⁷ (Figures S14 and S15) and that the binding of the alkyne-ester to Au^I(tcep)Cl is weak.³⁸ In addition to the binding of Au^ICl₂[–] to histidine, two further reversible current blockades were observed: at 4.8 ± 0.2 pA (with respect to P_H) with an average lifetime of 95 ± 4 ms (level 3), and at 2.2 ± 0.2 pA with an average lifetime of 241 ± 30 ms (level 2) (Figure 3a). As we anticipated observing only one reversible current blockade from the coordination of a linear, Au^I-**1** π -complex, the observation of two reversible current blockades prompted further investigation. These current levels were not observed with the WT₇ pore.

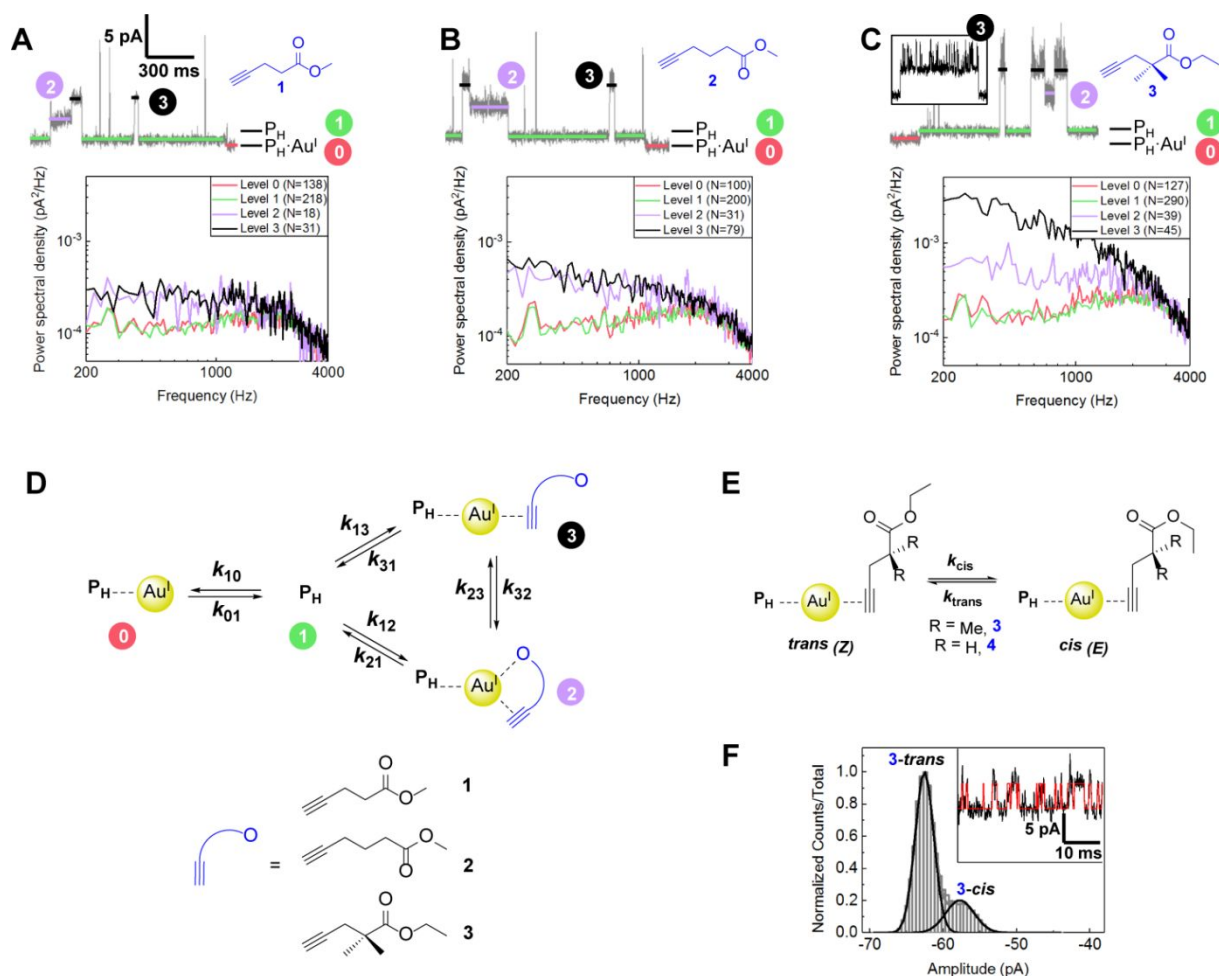


Figure 3. Detection of Au^I-alkyne complexes using the P_H pore. **(a – c)** Electrical current recordings (shown in grey with an idealised trace overlaid and color coded for each level) and noise analyses for the bound states of Au^I-coordinated alkyne-esters **1 – 3** to P_H (N = number of events). Inset in **(c)**: expanded view of level 3. Concentrations (Au^I(tcep)Cl and alkyne-ester added in a 1:1 stoichiometry: **1**, 50 μM; **2**, 50 μM; **3**, 50 μM. All traces are displayed on the same scale. Conditions: 2 M KCl, 10 mM MES, pH 6.1, 21 ± 1 °C, at an applied potential of –50 mV. **(d)** Kinetic model used to determine the rate constants of the observed transitions. **(e)** Proposed kinetic scheme describing the restricted rotation of alkyne esters **3** and **4** between the *trans* (Z) configuration and the *cis* (E) configuration. **(f)** All-points histogram of the current amplitudes in level 3 observed with **3**. Inset: idealised trace (QuB) of level 3 (red) overlaid on the recorded current trace (black).

Direct transitions from the unoccupied pore (level 1) to level 3 or level 2 and transitions between levels 3 and 2 were commonly observed, but transitions from the Au^I-occupied level (level 0) to levels 3 and 2 were rarely recorded (<1% of the total transitions) (Figure S16). We created a four-state model to describe the observed transitions (Figure 3d). The rate constants of the transitions between each state were determined by analysing idealised current traces with Hidden Markov modelling (QUB 2.0, Buffalo University) (Table 1). The association rate from level 1 to level 2 (corresponding to rate constant k_{12}) or level 3 (rate constant k_{13}) showed a first-order dependence on the concentration of the Au^I-**1** complex (Figure S17), while dissociation (rate constants k_{21} and k_{31}) was independent of the concentration, consistent with a bimolecular interaction between Au^I-**1** and P_H. The transitions between levels 3 and 2 (k_{23} and k_{32}) were concentration independent, suggesting that level 2 and level 3 arise from rearrangement of the coordination complex. As Au^I is known to form three-coordinate complexes³⁹ in addition to the more commonly observed linear, two-coordinate complexes, we tentatively assign levels 2 and 3 to two different coordination states: a linear, Au^I-**1** π -complex and a three-coordinate, Au^I complex chelated by the alkyne and ester groups (Figure 3d). We propose the three-coordinate, Au^I complex in order to account for our single-molecule observation that the transitions between level 2 and 3 are concentration independent; although this is an atypical binding motif, similar heterotopic and multidentate ligand binding to Au^I (Refs. 39-40) and Au^{III} (Ref. 41) have been reported. We did not observe binding of Au^I-ester (Figure S18) or Au^I-acid (Figure S19) complexes to P_H, indicating that coordination must be through the alkyne. Because the amplitude of the current block for an organic molecule depends approximately on how far it extends into the pore lumen,¹⁸ the chelate state was assigned to the smaller current blockade (level 2). Although this argument is the simplest and most chemically plausible, it encouraged us to investigate additional alkyne-ester binding activity to P_H.

The addition of a 1:1 mixture of Au^I(tcep)Cl and alkyne-ester **2** to the *trans* side of P_H produced current blockades and transitions similar to those produced by Au^I-**1** under the same experimental conditions (Figure 3b and Figure S21); **2** differs from **1** by only an additional carbon atom in the chain between the alkyne and ester group. We found that the rate constant of the transition from level 3 to level 2 (k_{32}), which is proposed to describe the chelation of Au^I by **2** to

form a 7-membered ring, was slower ($2.9 \pm 0.2 \text{ s}^{-1}$) than the formation of a 6-membered ring with Au^I and **1** ($4.4 \pm 0.4 \text{ s}^{-1}$) (Figure S22); similar small differences in ring-closing rates have been observed with platinum(II)-diamine chelate complexes.⁴² The opening of the 7-membered ring (k_{23}) formed with **2** was slightly faster ($8.1 \pm 0.4 \text{ s}^{-1}$) than the 6-membered ring with **1** ($6.4 \pm 0.5 \text{ s}^{-1}$). These results support our initial level 3 assignment as the Au^I-alkyne π -complex. Further, we determined the binding kinetics of Au^I-**3** to P_H (Figure 3c) (Figures S24 and S25). The dimethyl substituents of alkyne-ester **3** did not affect the rate of ring-opening ($k_{23} = 6.4 \pm 0.3 \text{ s}^{-1}$), as compared with alkyne-ester **1** (which forms the same chelate ring size), but slightly retarded the rate of ring formation ($k_{32} = 3.0 \pm 0.3 \text{ s}^{-1}$) as expected from the steric influence. Although the noise that arises from level 2, which is assigned as the Au^I-alkyne chelate complex, was similar among alkyne-esters **1** – **3**, we observed considerable noise in the amplitude of level 3 with Au^I-**3**, compared to Au^I-**1** and Au^I-**2** (Figure 3, a to c, bottom). We attribute this observation to the restricted rotation of the σ -bond within the ester group,⁴³ as it is the slowest rotating bond within the molecule (Figure 3e). By using Hidden Markov modelling (QUB 2.0, Buffalo University) to analyse the fluctuations of level 3 from Au^I-**3** as a two state system with transitions from the trans (*Z*) configuration to the cis (*E*) isomer (Figure 3f), we determined k_{cis} ($701 \pm 24 \text{ s}^{-1}$) and k_{trans} ($2193 \pm 75 \text{ s}^{-1}$) and calculated an *E* – *Z* free energy difference (ΔG°) of $0.52 \text{ kcal mol}^{-1}$ ($\Delta G^\circ = -RT \ln(k_{\text{cis}}/k_{\text{trans}})$), consistent with literature values.⁴⁴ We also prepared the ethyl ester of 4-pentynoic acid (**4**), which omits the dimethyl substituents of **3**, and observed a similar fluctuation in the amplitude of level 3 (Figure S26), and found faster k_{cis} ($1748 \pm 131 \text{ s}^{-1}$) and k_{trans} ($3274 \pm 237 \text{ s}^{-1}$) values, yielding a smaller *E* – *Z* free energy difference of $0.37 \text{ kcal mol}^{-1}$. This result suggests that the observed restricted rotation was a result of the ethyl ester group. The barrier to ester rotation is consistent with a linearly-coordinated, Au^I-alkyne π -complex to P_H, in support of our assignment of level 3. We also investigated the binding of *tert*-butyl propargyl carbonate to Au^I in the presence of P_H, in which the *tert*-butyl group sterically prevents chelation. We observed only a single current blockade, consistent with the formation of a simple π -complex and not a chelate (Figure S27). We could thus observe two different coordination modes of alkyne-esters **1** – **3** to Au^I with P_H and provide plausible assignments of the coordinating species.

Table 1. Rate constants for the interaction of Au^I-alkyne-esters **1** – **3** with the P_H Pore^[a]

Transition	1		2		3	
	Rate Constant	$n^{[b]}$	Rate Constant	$n^{[b]}$	Rate Constant	$n^{[b]}$
$k_{12} (\text{M}^{-1}\text{s}^{-1})$	$2.3 \pm 0.2 \times 10^2$	32	$2.5 \pm 0.1 \times 10^2$	35	$1.6 \pm 0.2 \times 10^2$	21
$k_{21} (\text{s}^{-1})$	4.2 ± 0.5	40	4.0 ± 0.6	42	4.1 ± 0.2	27
$k_{13} (\text{M}^{-1}\text{s}^{-1})$	$1.2 \pm 0.1 \times 10^3$	164	$1.15 \pm 0.09 \times 10^3$	193	$6.2 \pm 1.2 \times 10^2$	136
$k_{31} (\text{s}^{-1})$	10.5 ± 0.5	163	6.4 ± 0.6	190	11.1 ± 0.8	139
$k_{23} (\text{s}^{-1})$	6.4 ± 0.5	64	8.1 ± 0.4	99	6.4 ± 0.3	47
$k_{32} (\text{s}^{-1})$	4.4 ± 0.4	72	2.9 ± 0.2	104	3.0 ± 0.3	19

[a] Conditions: 2 M KCl, 10 mM MES, Chelex, pH 6.1, recorded at -50 mV and $21 \pm 1 \text{ }^\circ\text{C}$ ($n = 3$)

[b] n = number of events recorded in a selected experiment when 150 μM of both $\text{Au}^{\text{I}}(\text{tcep})\text{Cl}$ and alkyne ester were added to the *trans* compartment (refer to Figure 3)

Gold(I) catalysed cyclisation of acetylenic acids

The intramolecular cyclisation of acetylenic acids to produce enol lactones is catalysed by Au^{I} salts in organic solvent (Figure 1d).²³⁻²⁵ It has been proposed that the Au^{I} catalyst first coordinates to and activates the alkyne to promote the addition of the nucleophilic carboxylic acid. The corresponding vinyl- Au^{I} species, which has been isolated and visualised with X-ray crystallography,⁴⁵⁻⁴⁶ protodemetalates to yield the product and returns Au^{I} to the catalytic cycle. Accordingly, we found that the treatment of 4-pentynoic acid with $\text{Au}^{\text{I}}(\text{tcep})\text{Cl}$ at room temperature in water (buffered at pH 6.0, with and without 2M KCl) cleanly produced γ -methylene- γ -butyrolactone (Figures S28 and S29); these conditions were used because they were similar to the conditions employed in the nanoreactor experiments. The selective *exo*-dig cyclisation was also observed in organic media (Figure S30), consistent with literature observations. An *exo*-lactone was also produced catalytically from the similar acetylenic acid, 2,2-dimethyl-4-pentynoic acid, under the same aqueous conditions (Figure S31). As we were able to observe Au^{I} -alkyne binding to the P_{H} pore, we examined the intermediates in the catalytic cyclisation of acetylenic acids at the single-molecule level by using the nanoreactor approach.

When $\text{Au}^{\text{I}}(\text{tcep})\text{Cl}$ (300 μM) was added to the *trans* compartment of the bilayer apparatus containing 4-pentynoic acid (300 μM ; stoichiometric conditions) in 2 M KCl, 10 mM MES, pH 6.1, at an applied potential of -50 mV (Figure 4a), we observed three reversible blockades of P_{H} in addition to the open pore current (level 1) and the level with Au^{I} bound (level 0) (Figure 4b and Figures S32 and S33). Because the catalytic reaction proceeds in the *trans* compartment, P_{H} samples and records the intermediate Au^{I} -ligand species present in solution during the transformation. Transitions linking intermediates are observed as partial reaction cycles that occur on P_{H} , permitting construction of a reaction cycle and the associated kinetics. Performing the reaction under catalytic conditions (2 μM $\text{Au}^{\text{I}}(\text{tcep})\text{Cl}$ and 500 μM 4-pentynoic acid) did not yield sufficient binding events of Au^{I} -ligand intermediate species for statistical analysis. Further, when 30 μM (10 mol%) of $\text{Au}^{\text{I}}\text{Cl}_2^-$ was used as the catalyst with 300 μM 4-pentynoic acid, although the same reversible blockades were initially observed as seen with $\text{Au}^{\text{I}}(\text{tcep})\text{Cl}$, the ionic current through the nanopore quickly became blocked (Figure S34). We postulate that in the absence of a phosphine-coordinating ligand, aggregated Au^{I} and Au^{I} -ligand complexes form in solution and block the nanopore.¹⁷ The three current blockades suggested that there are three different Au^{I} -ligand species involved in the catalytic cycle ($n = 5$, independent experiments). We also recorded only three current blockades with the acetylenic acid 2,2-dimethyl-4-pentynoic acid ($n = 3$) (Figures S35 and S36). The largest blockade observed with 4-pentynoic acid (6.9 ± 0.3 pA) was

1
2 designated level 4 and had a life-time of 26 ± 1 ms. Smaller blockades of 5.2 ± 0.2 pA (level 3)
3
4 and 3.8 ± 0.2 pA (level 2) had longer life-times of 152 ± 8 ms and 205 ± 8 ms, respectively (Figure
5
6 4b). The number of events at each observed level decreased over the course of the reaction as 4-
7
8 pentynoic acid was converted to the enol lactone. The cumulative plots of the events fitted well to
9
10 exponential functions, as expected for a decay with a first-order dependence on each intermediate
11
12 (Figure 4c). As the time-dependence of the derivative of a cumulative events plot reflects the
13
14 change in concentration of an analyte with time (Supplementary Section 4.1),⁴⁷ and the initial
15
16 concentration of 4-pentynoic acid was known, we were able to determine a rate constant of $5.7 \pm$
17
18 $0.8 \times 10^{-4} \text{ s}^{-1}$ (the three intermediates gave the same rate constant and was averaged over five
19
20 experiments to determine the overall rate constant). The similar calculated rate constant for the
21
22 conversion of all of the observed intermediates (levels 4, 3 and 2) suggest that they interconvert at
23
24 rates considerably faster than the rate of product formation (see below). When the reaction was
25
26 followed by ^1H NMR under the same conditions in buffered D_2O (2 M KCl, 10 mM MES, p(DH)
27
28 6.1), a similar rate constant of $4.3 \pm 0.7 \times 10^{-4} \text{ s}^{-1}$ was obtained. A rate constant of $5.5 \pm 0.5 \times 10^{-4}$
29
30 s^{-1} was determined with 2,2-dimethyl-4-pentynoic acid (Figure S37).
31
32
33
34
35
36
37
38
39
40
41
42
43
44
45
46
47
48
49
50
51
52
53
54
55
56
57
58
59
60

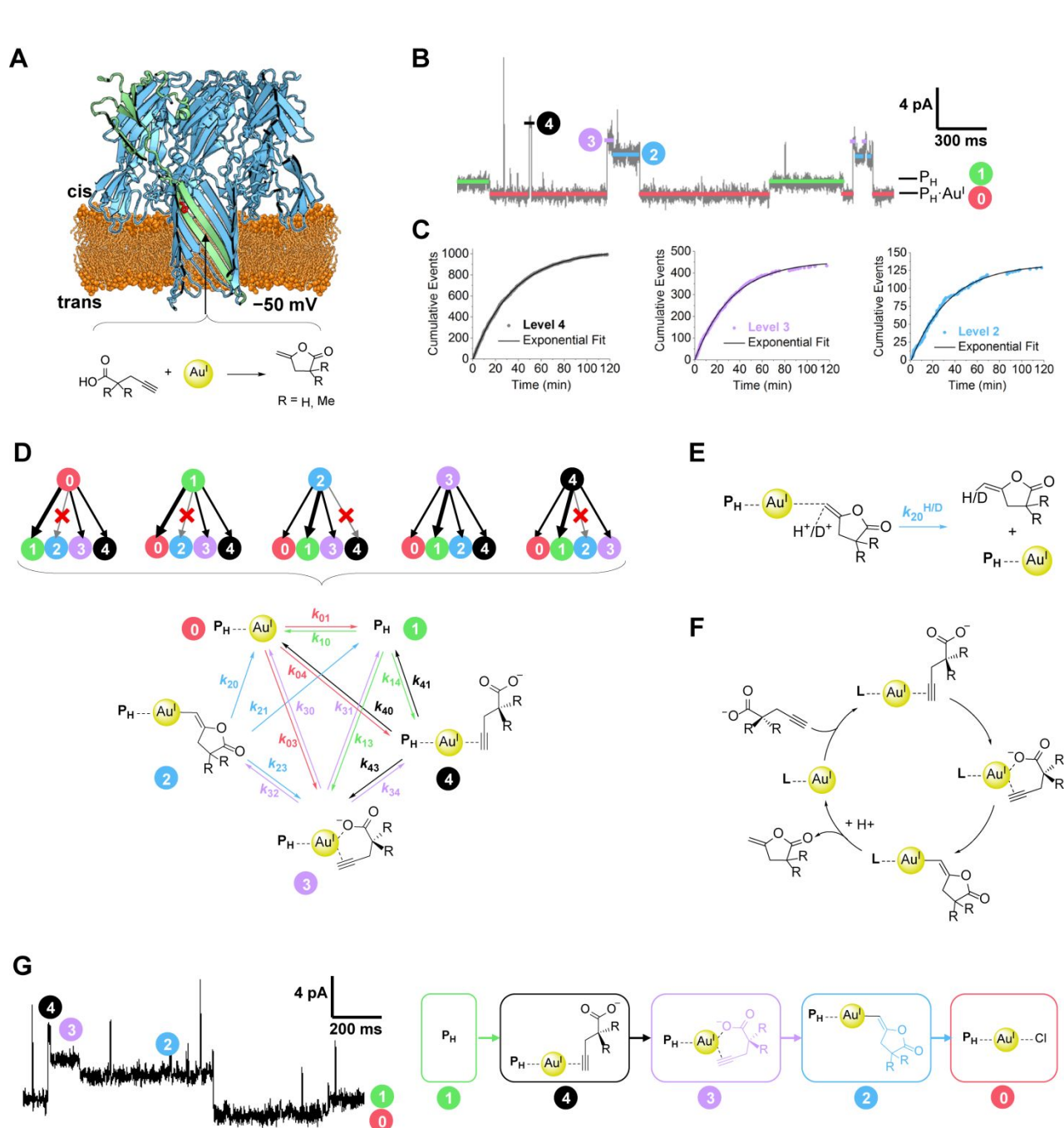


Figure 4. Single-molecule detection of catalytic intermediates. **(a)** A single P_H pore was incorporated into a planar lipid bilayer. An acetylenic acid was introduced to the trans compartment and the catalyst, $Au^I(tcep)Cl$, was added to initiate the reaction and catalytically produce the enol lactone. Conditions: 2 M KCl, 10 mM MES, pH 6.1, 21 ± 1 °C. **(b)** At an applied potential of -50 mV, analysis of the electrical recording during the reaction (grey) identified three current blocking events accessed from either the Au^I -bound state (level 0; red) or the unoccupied pore (level 1; green), which were assigned as level 4 (black), level 3 (purple), and level 2 (blue). **(c)** Cumulative plots of the reaction progress. The number of recorded events is proportional to the concentration of the intermediate Au^I -species and decreases over time as the substrate is converted to the product. **(d)** The transitions from each level observed in the electrical recordings were analysed to determine accessible transitions. This information was combined to create a kinetic model that describes the transitions between current levels. **(e)** Proposed kinetic scheme describing the proton-mediated demetallation step (k_{20}). **(f)** Our proposed catalytic cycle that describes the Au^I -catalysed cyclisation of acetylenic acids. **(g)** A recording of a complete catalytic cycle for the transformation of 4-pentynoic acid within P_H that transitions from levels 1 \rightarrow 4 \rightarrow 3 \rightarrow 2 \rightarrow 0. The chemical structure proposed for each level is shown.

We analysed the transitions from each level during the reaction of either 4-pentynoic acid or 2,2-dimethyl-4-pentynoic acid with Au^I (Figure 4d, top). We observed reversible transitions from

1
2 the Au^I-bound state (level 0) to level 1 (open pore), level 3 and 4. Similarly, reversible transitions
3 were observed from the open pore (level 1) to levels 0, 3 and 4. We also found that several
4 pathways were rarely observed ($\leq 2\%$ of the total transitions from that level): transitions from
5 either the open pore (level 1) or the Au^I-bound state (level 0) to level 2, and transitions between
6 levels 2 and 4. This revealed that level 2 was accessed **predominantly** from level 3. We collated
7 this information to construct a five-state model that describes these transitions (Figure 4d, bottom).
8 The rate constants associated with the transitions were determined by Hidden Markov modelling
9 (QUB 2.0, Buffalo University) (Table 2). Control experiments involving the addition of
10 Au^I(tcep)Cl and excess enol lactone to the *trans* compartment under the same conditions revealed
11 that the enol lactone product of the catalytic reaction did not coordinate to Au^I (Figure S38). **As we**
12 **also observed that level 2 does not occur from the coordination of a ligand, this suggested that**
13 **level 2 may be assigned to the vinyl-Au^I complex, which is the last intermediate in the proposed**
14 **catalytic cycle (Figure 1d). To better support this assignment,** and as the vinyl-Au^I species
15 protodemetallates to release the enol lactone and reintroduce Au^I into the catalytic cycle (Figure
16 4e), we repeated the reaction with 4-pentynoic and Au^I in D₂O solution ($n = 3$, independent
17 experiments) (Figures S39 and S40). We determined a rate constant of $3.8 \pm 1.3 \times 10^{-4} \text{ s}^{-1}$ (**using**
18 **300 μM of both 4-pentynoic acid and Au^I(tcep)Cl;** Figure S41), slower than that observed in H₂O
19 ($5.7 \pm 0.8 \times 10^{-4} \text{ s}^{-1}$, **performed with the same reactant concentrations**) and consistent with ¹H
20 NMR spectroscopy experiments in D₂O ($4.3 \pm 0.7 \times 10^{-4} \text{ s}^{-1}$); **we also extrapolated a product**
21 **formation rate constant of $\sim 7 \times 10^{-4} \text{ s}^{-1}$ from individual rate constants (Supplementary Section 4.3),**
22 **which agrees (roughly) with the bulk-observed rate constant.** We found a small solvent kinetic
23 hydrogen-deuterium isotope effect⁴⁸⁻⁵⁰ in the transition from level 2 to level 0, $k_{20}^{\text{H}} / k_{20}^{\text{D}} = 1.7$
24 (Table 2), and determined statistically insignificant ($P < 0.05$) isotope effects in the transitions
25 from level 4 and level 3 to level 0 ($k_{40}^{\text{H}} / k_{40}^{\text{D}} = 1.2$ and $k_{30}^{\text{H}} / k_{30}^{\text{D}} = 1.1$). This unambiguously
26 establishes that the transition from level 2 to level 0 is a proton mediated step, consistent with our
27 assignment of level 2 to the vinyl-Au^I species, which requires protonation for the product to
28 dissociate from the Au^I center. We also observed solvent kinetic isotope effects of < 1 for
29 transitions to the open pore (k_{01} , k_{21} , k_{31} , and k_{41}), coincident with isotope effects of > 1 for
30 transitions from the open pore (k_{10} , k_{13} and k_{14}) (Table 2). We postulate that these solvent isotope
31 effects result from the difference in hydrogen bond strength between H₂O and D₂O to the His-145
32 coordinating group.⁵¹

Table 2. Rate constants for the steps involved in the Au^I-catalysed conversion of acetylenic acids to enol lactones as determined with the P_H pore

Transition	4-pentynoic acid					2,2-dimethyl-4-pentynoic acid	
	H ₂ O ^[a] (<i>n</i> = 5)	<i>n</i> ^[b]	D ₂ O ^[c] (<i>n</i> = 3)	<i>n</i> ^[b]	<i>k</i> ^H / <i>k</i> ^D	H ₂ O ^[a] (<i>n</i> = 3)	<i>n</i> ^[b]
<i>k</i> ₀₁ (s ⁻¹)	1.5 ± 0.3	4137	3.9 ± 0.4	1899	0.40 ± 0.09	1.2 ± 0.2	4260
<i>k</i> ₀₃ (M ⁻¹ s ⁻¹)	1.0 ± 0.2 × 10 ³	190	1.3 ± 0.4 × 10 ³	99	0.83 ± 0.31	1.2 ± 0.2 × 10 ³	296
<i>k</i> ₀₄ (M ⁻¹ s ⁻¹)	5.8 ± 1.7 × 10 ²	120	4.3 ± 1.8 × 10 ²	31	1.33 ± 0.66	7.4 ± 0.3 × 10 ²	130
<i>k</i> ₁₀ (M ⁻¹ s ⁻¹)	2.8 ± 0.8 × 10 ³	4127	8.7 ± 1.2 × 10 ²	1899	3.25 ± 1.11	2.9 ± 0.1 × 10 ³	4276
<i>k</i> ₁₃ (M ⁻¹ s ⁻¹)	6.4 ± 2.5 × 10 ²	154	4.1 ± 0.9 × 10 ²	225	1.55 ± 0.71	7.6 ± 1.7 × 10 ³	174
<i>k</i> ₁₄ (M ⁻¹ s ⁻¹)	1.6 ± 0.5 × 10 ³	825	1.5 ± 0.5 × 10 ³	1022	1.08 ± 0.47	1.8 ± 0.6 × 10 ³	798
<i>k</i> ₂₀ (s ⁻¹)	0.8 ± 0.2	22	0.5 ± 0.1	10	1.73 ± 0.55	0.7 ± 0.1	24
<i>k</i> ₂₁ (s ⁻¹)	1.9 ± 0.7	52	4.2 ± 0.4	55	0.46 ± 0.17	1.8 ± 0.2	29
<i>k</i> ₂₃ (s ⁻¹)	1.0 ± 0.3	34	1.1 ± 0.1	13	0.85 ± 0.25	1.4 ± 0.2	51
<i>k</i> ₃₀ (s ⁻¹)	1.6 ± 0.4	156	1.5 ± 0.4	94	1.09 ± 0.41	1.7 ± 0.2	281
<i>k</i> ₃₁ (s ⁻¹)	3.0 ± 0.5	199	4.7 ± 0.3	230	0.64 ± 0.12	2.6 ± 0.3	182
<i>k</i> ₃₂ (s ⁻¹)	1.6 ± 0.5	25	1.5 ± 0.2	20	1.08 ± 0.40	1.8 ± 0.2	41
<i>k</i> ₃₄ (s ⁻¹)	0.5 ± 0.3	31	0.59 ± 0.09	27	0.83 ± 0.47	1.4 ± 0.2	124
<i>k</i> ₄₀ (s ⁻¹)	1.1 ± 0.2	130	0.9 ± 0.3	80	1.17 ± 0.44	1.9 ± 0.7	131
<i>k</i> ₄₁ (s ⁻¹)	26.4 ± 5.6	817	35.8 ± 2.4	1025	0.74 ± 0.16	25.2 ± 0.4	812
<i>k</i> ₄₃ (s ⁻¹)	1.1 ± 0.4	31	1.2 ± 0.4	29	0.86 ± 0.43	3.5 ± 0.3	109

[a] Conditions: 2 M KCl, 10 mM MES, Chelex, pH 6.1, recorded at -50 mV and 21 ± 1 °C

[b] *n* = number of events recorded in a selected experiment when 300 μM of both Au^I(tcep)Cl and acetylenic acid were added to the *trans* compartment (refer to Figure 4)

[c] Conditions: 2 M KCl, 10 mM MES, Chelex, p(DH) 6.1, recorded at -50 mV and 21 ± 1 °C

The life-times (τ_{off}) and amplitudes of levels 4 and 3 observed during the catalytic cycle were similar to the life-times of the binding events established with the unreactive alkyne-esters. We therefore assigned level 4 in the catalytic cycle to the Au^I-alkyne π -complex and level 3 to the formation of the alkyne-acid chelate (Figure 4d). We propose a catalytic cycle for the cyclisation of acetylenic acids in accord with our observations at the single-molecule level (Figure 4f). In the first step, the substrate coordinates to an open site on Au^I through the alkyne group to form a linear complex, activating the alkyne for nucleophilic attack. The Au^I center must then position the carboxylic acid to attack the activated alkyne. The resultant vinyl-Au^I species is then protonated to release the enol lactone irreversibly and allow Au^I to continue in the catalytic cycle. Although the identity of the **catalytic** intermediates cannot be proven definitively with our nanopore sensing approach, our catalytic model is the simplest and most chemically plausible scenario to describe the single-molecule experiments. Our strategy for the observation of catalysis at the single-molecule level relies on sampling the reaction as it proceeds in solution, observing the rates of transitions within the pore, and compiling this information to construct a catalytic cycle. We observed only a single event during a two hour electrical recording with 4-pentynoic acid that showed a sequence corresponding to a complete catalytic cycle without dissociation from the nanoreactor (i.e. levels 4 to 3 to 2 to 0) (Figure 4g). This is consistent with an expectation based on the probabilities of the different transitions (Supplementary Section 4.4). **Furthermore, the observation of the transitions from levels 4 and 3 (Au^I-alkyne intermediate species) to level 0 (the**

1
2 **Au^I-bound state) indicate that a substrate can dissociate from the catalytic Au^I center before**
3 **irreversible production of the enol lactone.**
4
5
6
7

8 **CONCLUSIONS**

9
10 In this study, we have monitored the Au^I-catalysed transformation of acetylenic acids into enol
11 lactones in real time, observing transitions at the single-molecule level and thereby establishing the
12 intermediates in the catalytic cycle. The nanoreactor approach has allowed direct observation of
13 the individual reaction intermediates and an analysis of the lifetimes and the allowed transitions of
14 each species. Therefore, the approach has advantages over ensemble measurements, which are
15 often limited to monitoring the rate-determining step. Although our approach is limited to the
16 investigation of reactions that occur in water, aqueous metal-catalysed reactions are of increasing
17 importance in bio-orthogonal and green chemistry. As we have been able to discriminate between
18 enantiomeric amino acids by binding to a copper(II) complex within a nanopore,⁴⁷ we believe our
19 approach may be adapted to identify the handedness of a chiral intermediate involved in a metal-
20 catalysed reaction. We anticipate that the observation of the reactions of ligands on catalytically
21 active metal centres bound within a nanopore will shed light on additional multistep reaction
22 mechanisms.
23
24
25
26
27
28
29
30
31
32
33

34 **ASSOCIATED CONTENT**

35 **Supporting Information**

36
37 The Supporting Information for this paper is available free of charge on the ACS Publications
38 website.
39
40

41
42 Synthetic details, characterisation data, and single-molecule analyses.
43
44
45

46 **AUTHOR INFORMATION**

47 **Corresponding Author**

48
49 *E-mail: hagan.bayley@chem.ox.ac.uk
50

51 **ORCID**

52
53 Hagan Bayley : 0000-0003-2499-6116
54

55 **Notes**

56
57 The authors declare no competing financial interest.
58
59
60

ACKNOWLEDGEMENTS

This work was supported by a European Research Council Advanced Grant (COSIMO). Y.Q. was the recipient of China Scholarship Council-University of Oxford Scholarship.

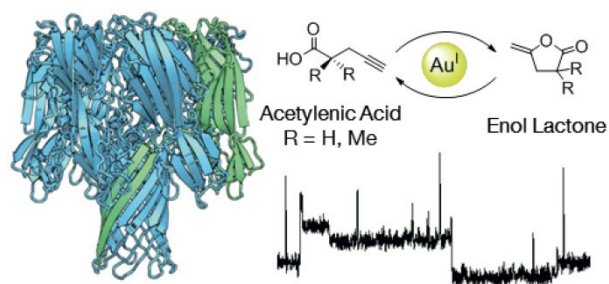
REFERENCES

1. Magano, J.; Dunetz, J. R., Large-scale applications of transition metal-catalyzed couplings for the synthesis of pharmaceuticals. *Chem. Rev.* **2011**, *111* (3), 2177-2250.
2. Beller, M.; Blaser, H. U.; Eds., *Organometallics as Catalysts in the Fine Chemical Industry*, vol 42 of *Topics in Organometallic Chemistry*. Springer, Berlin, Heidelberg: 2012.
3. Topczewski, J. J.; Cabrera, P. J.; Saper, N. I.; Sanford, M. S., Palladium-catalysed transannular C–H functionalization of alicyclic amines. *Nature* **2016**, *531* (7593), 220-224.
4. Thomas, A. A.; Denmark, S. E., Pre-transmetalation intermediates in the Suzuki-Miyaura reaction revealed: the missing link. *Science* **2016**, *352* (6283), 329-332.
5. Zhang, M.; Frei, H., Water Oxidation Mechanisms of Metal Oxide Catalysts by Vibrational Spectroscopy of Transient Intermediates. *Annu. Rev. Phys. Chem.* **2017**, *68* (1), 209-231.
6. Malta, G.; Kondrat, S. A.; Freakley, S. J.; Davies, C. J.; Lu, L.; Dawson, S.; Thetford, A.; Gibson, E. K.; Morgan, D. J.; Jones, W.; Wells, P. P.; Johnston, P.; Catlow, C. R. A.; Kiely, C. J.; Hutchings, G. J., Identification of single-site gold catalysis in acetylene hydrochlorination. *Science* **2017**, *355* (6332), 1399-1403.
7. Attar, A. R.; Bhattacharjee, A.; Pemmaraju, C. D.; Schnorr, K.; Closser, K. D.; Prendergast, D.; Leone, S. R., Femtosecond x-ray spectroscopy of an electrocyclic ring-opening reaction. *Science* **2017**, *356* (6333), 54-59.
8. Schuler, B.; Fatayer, S.; Mohn, F.; Moll, N.; Pavliček, N.; Meyer, G.; Peña, D.; Gross, L., Reversible Bergman cyclization by atomic manipulation. *Nat. Chem.* **2016**, *8* (3), 220-224.
9. Riss, A.; Paz, A. P.; Wickenburg, S.; Tsai, H.-Z.; De Oteyza, D. G.; Bradley, A. J.; Ugeda, M. M.; Gorman, P.; Jung, H. S.; Crommie, M. F.; Rubio, A.; Fischer, F. R., Imaging single-molecule reaction intermediates stabilized by surface dissipation and entropy. *Nat. Chem.* **2016**, *8*, 678.
10. van Schrojenstein Lantman, E. M.; Deckert-Gaudig, T.; Mank, A. J. G.; Deckert, V.; Weckhuysen, B. M., Catalytic processes monitored at the nanoscale with tip-enhanced Raman spectroscopy. *Nat. Nanotech.* **2012**, *7*, 583.
11. Arina, R.; Carolin, L.; Marcel, W.; Kristin, G. m.; Anton, K.; Frank, M.; Alexander, S.; Oliver, T.; Gregor, J.; Dirk-Peter, H., Distinguishing Alternative Reaction Pathways by Single-Molecule Fluorescence Spectroscopy. *Angew. Chem. Int. Ed.* **2013**, *52* (24), 6322-6325.
12. Ng, J. D.; Upadhyay, S. P.; Marquard, A. N.; Lupo, K. M.; Hinton, D. A.; Padilla, N. A.; Bates, D. M.; Goldsmith, R. H., Single-molecule investigation of initiation dynamics of an organometallic catalyst. *J. Am. Chem. Soc.* **2016**, *138* (11), 3876-3883.
13. Liu, C.; Kubo, K.; Wang, E.; Han, K.-S.; Yang, F.; Chen, G.; Escobedo, F. A.; Coates, G. W.; Chen, P., Single polymer growth dynamics. *Science* **2017**, *358* (6361), 352-355.
14. Easter, Q. T.; Blum, S. A., Single Turnover at Molecular Polymerization Catalysts Reveals Spatiotemporally Resolved Reactions. *Angew. Chem. Int. Ed.* **2017**, *56* (44), 13772-13775.
15. Song, L.; Hobaugh, M. R.; Shustak, C.; Cheley, S.; Bayley, H.; Gouaux, J. E., Structure of Staphylococcal α -Hemolysin, a Heptameric Transmembrane Pore. *Science* **1996**, *274* (5294), 1859-1865.
16. Bayley, H.; Luchian, T.; Shin, S. H.; Steffensen, M. B., "Single-molecule covalent chemistry in a protein nanoreactor" in *Single Molecules and Nanotechnology* (Eds Rigler, R.; Vogel, H.) Springer: 2008, 251–277.

17. Choi, L.-S.; Mach, T.; Bayley, H., Rates and stoichiometries of metal ion probes of cysteine residues within ion channels. *Biophys. J.* **2013**, *105* (2), 356-364.
18. Boersma, A. J.; Brain, K. L.; Bayley, H., Real-time stochastic detection of multiple neurotransmitters with a protein nanopore. *ACS Nano* **2012**, *6* (6), 5304-5308.
19. Lu, S.; Li, W.-W.; Rotem, D.; Mikhailova, E.; Bayley, H., A primary hydrogen–deuterium isotope effect observed at the single-molecule level. *Nat. Chem.* **2010**, *2* (11), 921-928.
20. Ren, H.; Cheyne, C. G.; Fleming, A. M.; Burrows, C. J.; White, H. S., Single-Molecule Titration in a Protein Nanoreactor Reveals the Protonation/Deprotonation Mechanism of a C:C Mismatch in DNA. *J. Am. Chem. Soc.* **2018**, *140* (15), 5153-5160.
21. Lee, J.; Bayley, H., Semisynthetic protein nanoreactor for single-molecule chemistry. *Proc. Natl. Acad. Sci. U.S.A.* **2015**, *112* (45), 13768-13773.
22. Pulcu, G. S.; Mikhailova, E.; Choi, L.-S.; Bayley, H., Continuous observation of the stochastic motion of an individual small-molecule walker. *Nat. Nanotech.* **2015**, *10* (1), 76-83.
23. Genin, E.; Toullec, P. Y.; Antoniotti, S.; Brancour, C.; Genêt, J.-P.; Michelet, V., Room temperature Au(I)-catalyzed exo-selective cycloisomerization of acetylenic acids: an entry to functionalized γ -lactones. *J. Am. Chem. Soc.* **2006**, *128* (10), 3112-3113.
24. Harkat, H.; Dembelé, A. Y.; Weibel, J.-M.; Blanc, A.; Pale, P., Cyclization of alkynoic acids with gold catalysts: a surprising dichotomy between Au^I and Au^{III}. *Tetrahedron* **2009**, *65* (9), 1871-1879.
25. Jimenez-Nunez, E.; Echavarren, A. M., Molecular diversity through gold catalysis with alkynes. *Chem. Comm.* **2007**, (4), 333-346.
26. Maglia, G.; Restrepo, M. R.; Mikhailova, E.; Bayley, H., Enhanced translocation of single DNA molecules through α -hemolysin nanopores by manipulation of internal charge. *Proc. Natl. Acad. Sci. U.S.A.* **2008**, *105* (50), 19720-19725.
27. Pan, P.; Wood, S. A., Gold-chloride complexes in very acidic aqueous solutions and at temperatures 25–300 °C: A laser Raman spectroscopic study. *Geochim. Cosmochim. Acta* **1991**, *55* (8), 2365-2371.
28. Gammons, C. H.; Yu, Y.; Williams-Jones, A. E., The disproportionation of gold(I) chloride complexes at 25 to 200°C. *Geochim. Cosmochim. Acta* **1997**, *61* (10), 1971-1983.
29. Hashmi, A. S. K.; Hutchings, G. J., Gold catalysis. *Angew. Chem. Int. Ed.* **2006**, *45* (47), 7896-7936.
30. Widenhoefer, R. A.; Han, X., Gold-catalyzed hydroamination of C–C multiple bonds. *Eur. J. Org. Chem.* **2006**, *2006* (20), 4555-4563.
31. Zhang, L.; Sun, J.; Kozmin, S. A., Gold and platinum catalysis of enyne cycloisomerization. *Adv. Synth. Catal.* **2006**, *348* (16-17), 2271-2296.
32. Jones, P. G.; Williams, A. F., Structure and bonding in gold(I) compounds. Part 1. The trans influence in linear complexes. *J. Chem. Soc., Dalton Trans.* **1977**, (15), 1430-1434.
33. Shapiro, N. D.; Toste, F. D., Synthesis and structural characterization of isolable phosphine coinage metal π -complexes. *Proc. Natl. Acad. Sci. U.S.A.* **2008**, *105* (8), 2779-2782.
34. Flügge, S.; Anoop, A.; Goddard, R.; Thiel, W.; Fürstner, A., Structure and bonding in neutral and cationic 14-electron gold alkyne π complexes. *Chem. Eur. J.* **2009**, *15* (34), 8558-8565.
35. Liu, L.-P.; Hammond, G. B., Recent advances in the isolation and reactivity of organogold complexes. *Chem. Soc. Rev.* **2012**, *41* (8), 3129-3139.
36. Goodwin, J. A.; Aponick, A., Regioselectivity in the Au-catalyzed hydration and hydroalkoxylation of alkynes. *Chem. Comm.* **2015**, *51* (42), 8730-8741.
37. Corma, A.; Leyva-Pérez, A.; Sabater, M. J., Gold-catalyzed carbon–heteroatom bond-forming reactions. *Chem. Rev.* **2011**, *111* (3), 1657-1712.
38. Brooner, R. E. M.; Widenhoefer, R. A., Cationic, Two-Coordinate Gold π Complexes. *Angew. Chem. Int. Ed.* **2013**, *52* (45), 11714-11724.
39. Gimeno, M. C.; Laguna, A., Three- and four-coordinate gold(I) complexes. *Chem. Rev.* **1997**, *97* (3), 511-522.

- 1
2
3
4
5
6
7
8
9
10
11
12
13
14
15
16
17
18
19
20
21
22
23
24
25
26
27
28
29
30
31
32
33
34
35
36
37
38
39
40
41
42
43
44
45
46
47
48
49
50
51
52
53
54
55
56
57
58
59
60
40. Johnson, A.; Gimeno, M. C., Synthesis of Propargyl-Functionalized NHC Gold Complexes. *Organometallics* **2017**, *36* (7), 1278-1286.
41. Luca, R.; Julio, F.-C.; Gabriele, A.; Isabelle, C.; M., B. P. H.; Manfred, B., Gold(III) Alkyne Complexes: Bonding and Reaction Pathways. *Angew. Chem. Int. Ed.* **2017**, *56* (44), 13861-13865.
42. Romeo, R.; Lanza, S.; Tobe, M. L., Kinetics of the chelate effect. Ring closing and ring opening in cis-dichloro(dimethyl sulfoxido)(2-aminoethylammonium)platinum(II) chloride. *Inorg. Chem.* **1977**, *16* (4), 785-790.
43. Dugave, C.; Demange, L., Cis–trans isomerization of organic molecules and biomolecules: implications and applications. *Chem. Rev.* **2003**, *103* (7), 2475-2532.
44. Pawar, D. M.; Khalil, A. A.; Hooks, D. R.; Collins, K.; Elliott, T.; Stafford, J.; Smith, L.; Noe, E. A., E and Z conformations of esters, thiol esters, and amides. *J. Am. Chem. Soc.* **1998**, *120* (9), 2108-2112.
45. Hashmi, A. S. K.; Ramamurthi, T. D.; Rominger, F., On the trapping of vinylgold intermediates. *Adv. Synth. Catal.* **2010**, *352* (6), 971-975.
46. Egorova, O. A.; Seo, H.; Kim, Y.; Moon, D.; Rhee, Y. M.; Ahn, K. H., Characterization of vinylgold intermediates: gold-mediated cyclization of acetylenic amides. *Angew. Chem. Int. Ed.* **2011**, *50* (48), 11446-11450.
47. Boersma, A. J.; Bayley, H., Continuous stochastic detection of amino acid enantiomers with a protein nanopore. *Angew. Chem. Int. Ed.* **2012**, *51* (38), 9606-9609.
48. Gandour, R. D.; Pivert, M. A.; Kelley, E. L.; Minor, B. D.; Spencer, R.; Ingraham, R. H.; Spindler, S. J., Solvent isotope effects in intramolecular catalysis: acyl transfer reactions of 4-nitrophenyl 5-nitrosalicylate in aqueous tris buffer. *Bioorg. Chem.* **1979**, *8* (1), 45-58.
49. Sim, Y.-L.; Ariffin, A.; Khan, M. N., Kinetics and mechanism of large rate enhancement in the alkaline hydrolysis of N'-morpholino-N-(2'-methoxyphenyl)phthalamide. *J. Org. Chem.* **2008**, *73* (10), 3730-3737.
50. Belafdal, O.; Bergon, M.; Calmon, M.; Calmon, J. P., Kinetics and mechanisms of cyclization in acidic media of N-[(3,5-dichloroanilino)carbonyl]-N-[(isopropylamino)carbonyl]glycine to hydantoins: iprodione and its isomer. *J. Org. Chem.* **1989**, *54* (17), 4193-4198.
51. Soper, A. K.; Benmore, C. J., Quantum differences between heavy and light water. *Phys. Rev. Lett.* **2008**, *101* (6), 065502.

Table of Contents Graphic



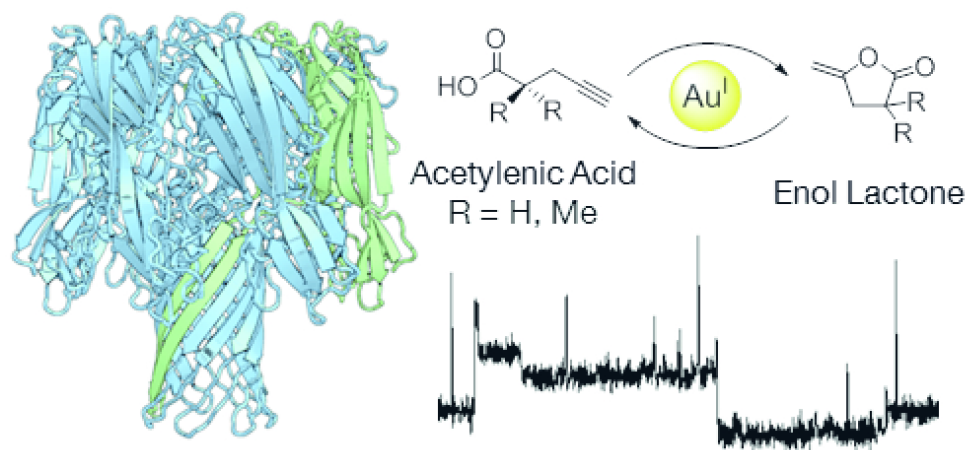


Table of Contents Graphic

85x39mm (300 x 300 DPI)

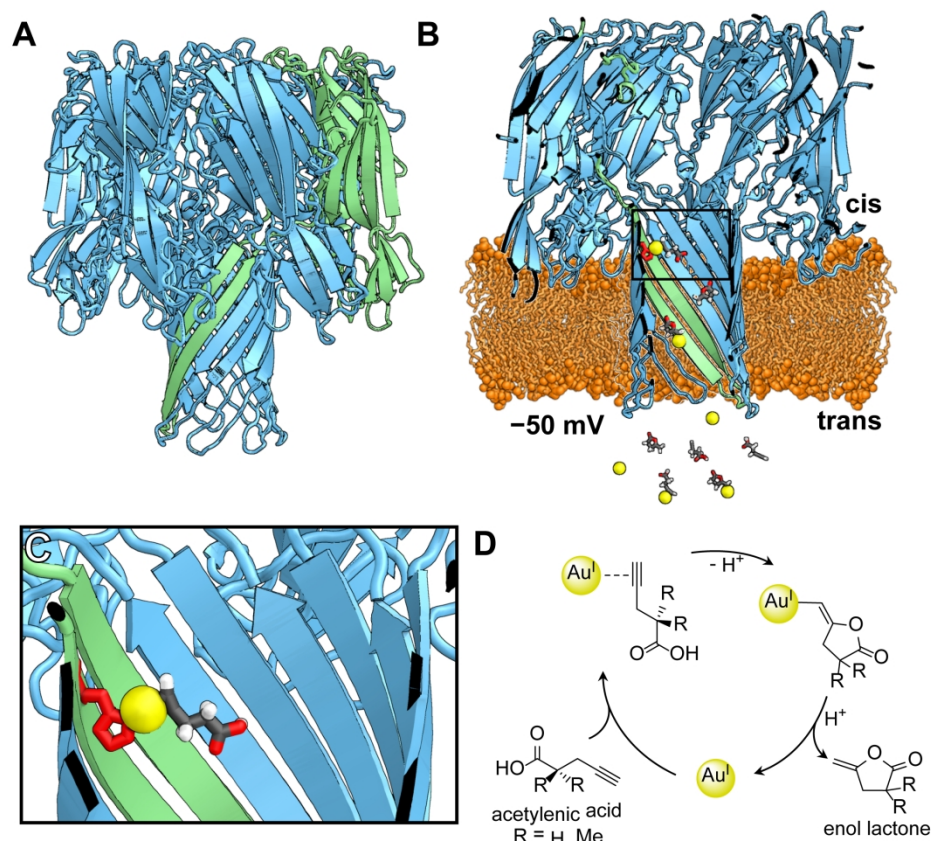


Figure 1. The PH α HL pore: a nanoreactor for the investigation of Au^{I} catalysis. (a) WT α HL (PDB code 7AHL) is a mushroom-shaped transmembrane protein pore comprising seven identical subunits. A side view of the ribbon structure shown with one of the subunits highlighted in green. (b) A sagittal section of the engineered α HL pore, PH, embedded in a planar lipid bilayer (orange) for single-channel electrical recording. PH contains one subunit with a histidine substitution at position 145 (red in stick representation). The side chain of His-145 points into the lumen of the transmembrane β barrel and can coordinate metal-ligand complexes from solution, entering from the trans compartment. (c) An expanded view around His-145, with bound 4-pentynoic acid: Au^{I} (yellow sphere), 4-pentynoic acid (stick representation: carbon, grey; hydrogen, white; oxygen, red). (d) The proposed catalytic cycle for transformation of an acetylenic acid to an enol lactone.

211x179mm (300 x 300 DPI)

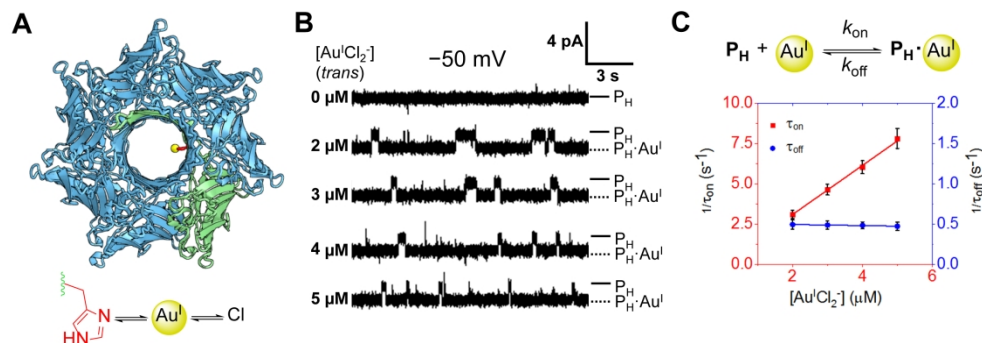


Figure 2. The PH pore binds AuI. (a) Ribbon representation of the PH pore viewed from the bottom of the β barrel. The single histidine side chain (red) binds AuI (yellow sphere) reversibly. (b) Single-channel recordings at -50 mV with 2 M KCl, 10 mM MES (pH 6.1) in both compartments, and 0 to 5 μ M AuICl₂⁻ in the trans compartment. The two current levels correspond to the unoccupied pore (PH) and to the pore with AuICl₂⁻ bound to the histidine residue (PH·AuI). (c) Proposed kinetic scheme describing AuI binding to the PH pore and plots of the reciprocals of the mean inter-event intervals (τ_{on}) and the dwell times of AuI (τ_{off}) versus the AuICl₂⁻ concentration.

252x89mm (300 x 300 DPI)

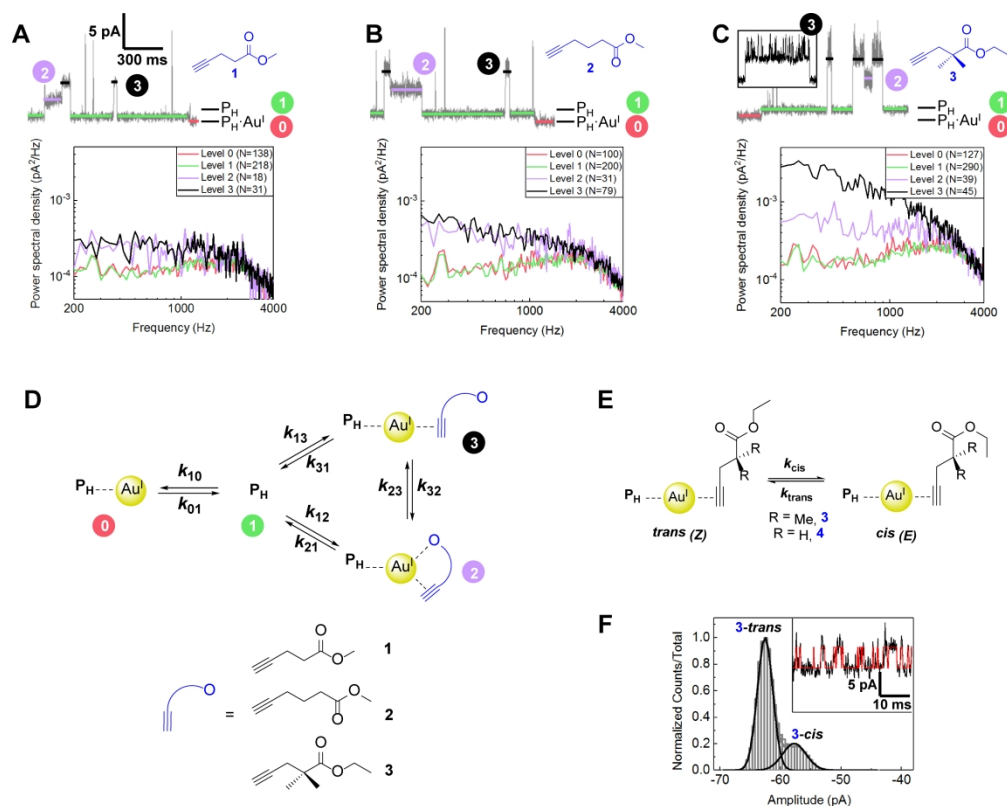


Figure 3. Detection of AuI-alkyne complexes using the PH pore. (a – c) Electrical current recordings (shown in grey with an idealised trace overlaid and color coded for each level) and noise analyses for the bound states of AuI-coordinated alkyne-esters 1 – 3 to PH (N = number of events). Inset in (c): expanded view of level 3. Concentrations (AuI(tcep)Cl and alkyne-ester added in a 1:1 stoichiometry: 1, 50 μ M; 2, 50 μ M; 3, 50 μ M. All traces are displayed on the same scale. Conditions: 2 M KCl, 10 mM MES, pH 6.1, 21 ± 1 $^{\circ}$ C, at an applied potential of -50 mV. (d) Kinetic model used to determine the rate constants of the observed transitions. (e) Proposed kinetic scheme describing the restricted rotation of alkyne esters 3 and 4 between the trans (Z) configuration and the cis (E) configuration. (f) All-points histogram of the current amplitudes in level 3 observed with 3. Inset: idealised trace (QuB) of level 3 (red) overlaid on the recorded current trace (black).

281x224mm (300 x 300 DPI)

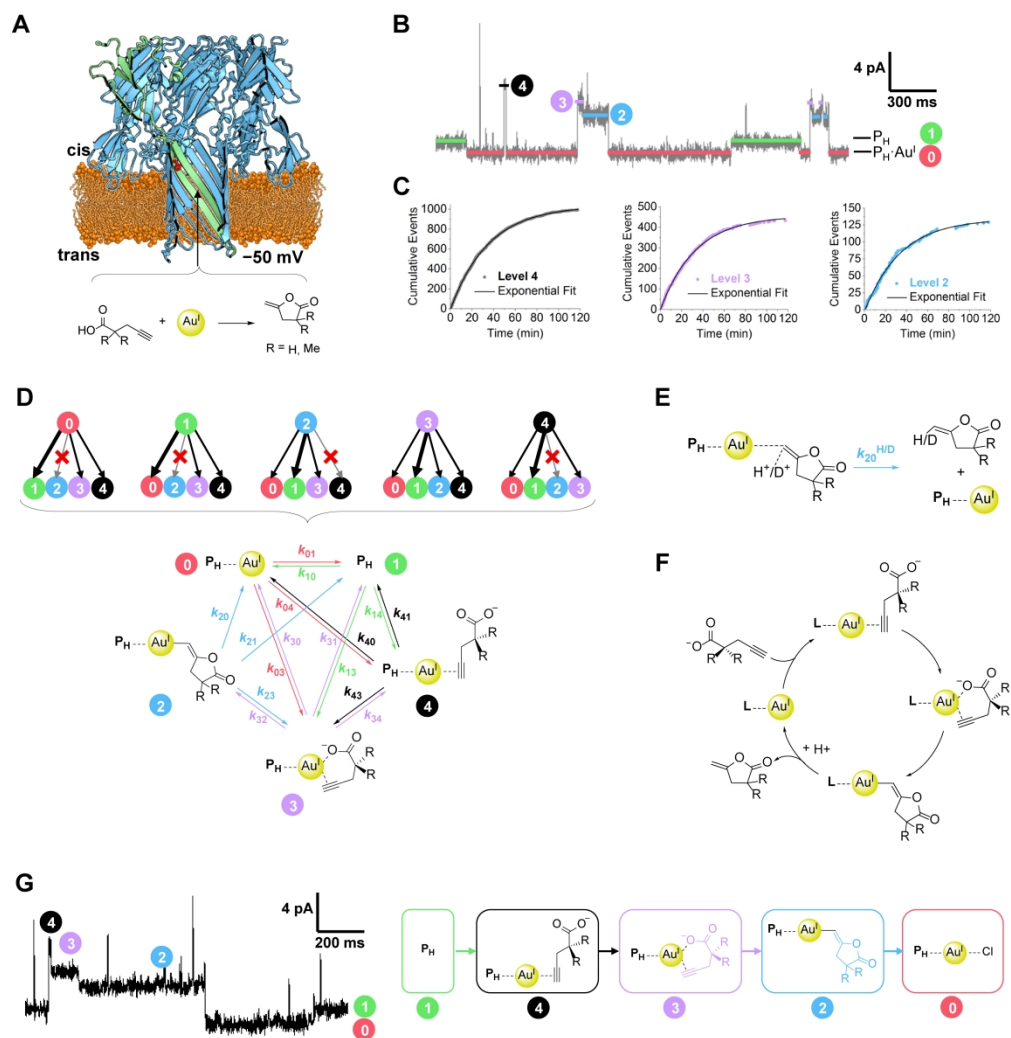


Figure 4. Single-molecule detection of catalytic intermediates. (a) A single PH pore was incorporated into a planar lipid bilayer. An acetylenic acid was introduced to the trans compartment and the catalyst, AuI(tcep)Cl, was added to initiate the reaction and catalytically produce the enol lactone. Conditions: 2 M KCl, 10 mM MES, pH 6.1, 21 ± 1 °C. (b) At an applied potential of -50 mV, analysis of the electrical recording during the reaction (grey) identified three current blocking events accessed from either the AuI-bound state (level 0; red) or the unoccupied pore (level 1; green), which were assigned as level 4 (black), level 3 (purple), and level 2 (blue). (c) Cumulative plots of the reaction progress. The number of recorded events is proportional to the concentration of the intermediate AuI-species and decreases over time as the substrate is converted to the product. (d) The transitions from each level observed in the electrical recordings were analysed to determine accessible transitions. This information was combined to create a kinetic model that describes the transitions between current levels. (e) Proposed kinetic scheme describing the proton-mediated demetallation step (k_{20}). (f) Our proposed catalytic cycle that describes the AuI-catalysed cyclisation of acetylenic acids. (g) A recording of a complete catalytic cycle for the transformation of 4-pentynoic acid within PH that transitions from levels 1 \rightarrow 4 \rightarrow 3 \rightarrow 2 \rightarrow 0. The chemical structure proposed for each level is shown.

284x298mm (300 x 300 DPI)